

(1976).

¹¹E. Clementi and C. Roetti, *At. Data Nucl. Data Tables* **14**, 177 (1974).¹²R. J. Fortner, P. H. Woerlee, S. Doorn, Th. P.Hoogkamer, and F. W. Saris, *Phys. Rev. Lett.* **39**, 1322 (1977).¹³E. G. Bøving, *J. Phys. B* **10**, L63 (1977); P. H. Woerlee *et al.*, to be published.

Measurements of the Parametric Decay of Co-Laser Radiation into Plasma Waves at Quarter-Critical Density Using Ruby-Laser Thomson Scattering

J. J. Schuss,^(a) T. K. Chu, and L. C. Johnson*Plasma Physics Laboratory, Princeton University, Princeton, New Jersey 08540*

(Received 28 October 1977)

We report the results of small-angle ruby-laser Thomson-scattering measurements of the parametric excitation of plasma waves by CO₂-laser radiation at quarter-critical density in a laser-heated gas-target plasma. From supplementary data obtained from interferometry and large-angle ruby-laser scattering we infer that the threshold conditions for a convective decay are satisfied.

It has long been recognized that parametric processes in the underdense plasma will crucially affect the prospects for both laser-pellet fusion and laser-heated solenoid fusion. Numerous experiments have been carried out studying Brillouin backscattered light¹⁻³; absorption instabilities at quarter-critical density have been observed by the detection of $\frac{3}{2}\omega_0$ harmonically generated light.⁴⁻⁵ Langmuir turbulence driven by a CO₂-laser pump wave near critical density has been observed by incoherent ruby-laser scattering-in a dense-plasma focus.⁶ In this Letter we report the first direct ruby-laser Thomson scattering observation of the parametric decay of laser light into plasma waves at quarter-critical density in a CO₂-laser-heated gas-target plasma. This diagnostic is supplemented by large-angle Thomson scattering and ruby-laser interferometry, which obtain n_e , T_e , and the gradient length L at the time the instability occurs. This combination of ruby-laser Thomson scattering on a gas-target plasma offers substantial advantages over other diagnostics in determining the level and localization of parametric instabilities; this is especially true when the direct products of the instability do not exit the plasma, as in the two-plasmon decay to be discussed here.

The experiment is schematically depicted in Fig. 1. A 40-J 130-nsec FWHM (full width at half-maximum) TEA (transversely excited atmosphere) CO₂-laser beam is focused onto a hydrogen gas jet exiting from a 47-Torr pressurized chamber through a 6-mm-diam orifice. The neutral-gas density gradient formed by this gas jet prevents the formation of a backward-propagating

ionization wave and allows the penetration of the laser light into the plasma interior.⁷ The plasma which is created at the CO₂-laser focal spot grows in the axial direction until it reaches the ruby-laser scattering volume approximately 10 nsec after breakdown. Thomson scattering is accomplished by focusing the output of a 2-J 3-

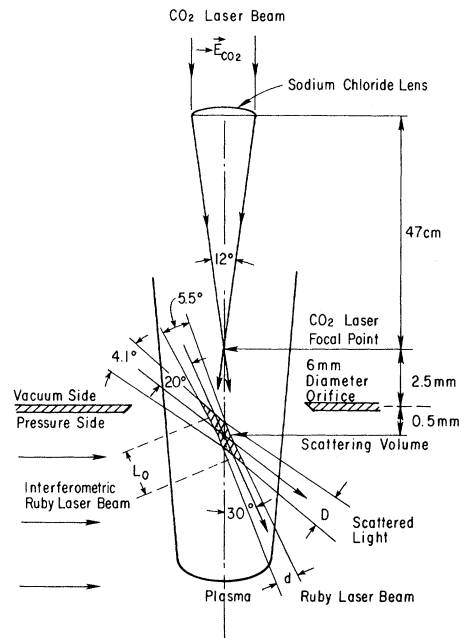


FIG. 1. Geometry of the small-angle scattering experiment. $L_0 \approx 0.66$ mm, $d < 0.25$ mm, and $D \approx 0.23$ mm. For large-angle scattering, the angle between the ruby-laser beam and collected light is changed to 150° , $L_0 \approx 0.66$ mm, and $D \approx 0.33$ mm.

nsec FWHM ruby-laser beam to a spot size less than 0.25 mm at the scattering volume, as shown in Fig. 1. The light that is Thomson scattered at a 20° angle relative to the ruby-laser beam is then collected and directed into a sixteen-channel spectrometer for analysis. This geometry selects a $\Delta\mathbf{k}$ which approximately bisects the angle between the \mathbf{k}_0 and \mathbf{E}_0 of the CO_2 -laser pump wave; this orientation of $\Delta\mathbf{k}$ maximizes the growth rate of the two-plasmon decay when $\Delta\omega \approx \omega_0/2$.⁸ Large-angle scattering is accomplished by collecting the radiation Thomson scattered by the plasma at a 150° angle relative to the ruby-laser beam. The remainder of the geometry and the scattering volume remain the same as in 20° scattering. Both 150° and 20° scattering are supplemented by simultaneous ruby-laser interferometry, which is accomplished by splitting off a small component of the ruby-laser beam and using it to illuminate a Mach-Zehnder interferometer. The time of breakdown is determined by a photon-drag detector that monitors the initiation of plasma self-focusing of the CO_2 laser light.⁹

Each frequency channel of the spectrometer consists of a single low-loss optical fiber whose light-transmitting core of $55 \mu\text{m}$ diameter has an attenuation of 5 dB/km at $0.82 \mu\text{m}^{10}$; the channels have an average spectral width of 11 \AA and separation of 25 \AA . The fibers are made successively longer in proportion to their frequency shift and then rejoined and focused onto a single photomultiplier tube; the average time separation is 18 nsec/channel. Since the Thomson scattered light has a time duration of approximately 5 nsec, the output of the photomultiplier consists of a series of sharp spikes, each spike being a measure of the light collected by its respective channel. This output signal can then be reconstructed into the incident spectrum.

Typical raw data obtained near the time the instability occurs are shown in Fig. 2. Each channel is identified by its delay relative to the ruby-laser monitor signal. The first channel is set at $\lambda = 6943 + 13 \text{ \AA}$ and channel No. 10 is set at $\lambda = 6943 + 235 \text{ \AA}$, the frequency of ruby-laser light scattered by the two-plasmon parametric decay. For small-angle scattering at quarter-critical density with $T_e \approx 50 \text{ eV}$, $\alpha \equiv (\Delta k \lambda_D)^{-1} \approx 10.1$, and each scattering spectrum is composed of a sharp spike at $\Delta\omega \approx \omega_{pe}$ as shown in Fig. 2(a). In the absence of the instability, small-angle scattering yields similarly sharply peaked spectra at $\Delta\omega = \omega_{pe}$, but the level of the peak is reduced by

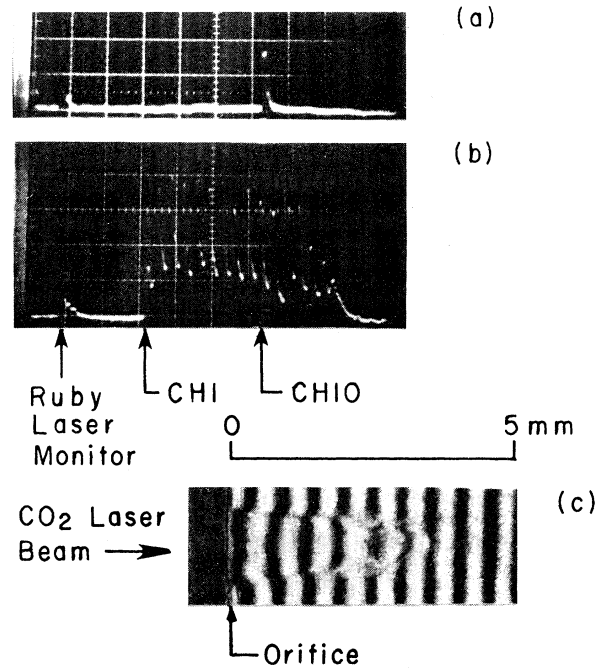


FIG. 2. Typical raw data. (a) 20° scattering spectrum exhibiting the instability and (b) is a typical 150° spectrum (1 division is 50 nsec). The photomultiplier gain in (a) is a factor of 8.8 less than in (b). The interferogram in (c) was taken simultaneously with an observation of the instability.

more than a factor of 10 from the unstable case; nevertheless, the signal-to-noise ratio is still better than 10:1, permitting a measurement of the thermal level of fluctuations in the absence of the instability. Figure 2(b) shows a typical large-angle spectrum taken at a time approximately 2 nsec after the instability is expected to occur; in this case $n_e \approx 1.3 \times 10^{18} \text{ cm}^{-3}$ and $T_e \approx 45 \text{ eV}$, yielding $\alpha = 1.31$. These broad large-angle spectra can be computer fitted to obtain n_e and T_e at the location of the scattering volume. A typical interferogram taken simultaneously with an instability observation is shown in Fig. 2(c). An Abel inversion of the interferogram reveals a 1-mm-diam plasma with a relatively flat low-density inner core of approximately 0.6 mm diam.

Figure 3 shows the $n_e(t)$ and $T_e(t)$ determined by both 150° and 20° scattering at the location of the scattering volume. The solid line is an approximate analytical fit to the observed time behaviors. A rapid time variation of $T = |(1/n)(dn/dt)|^{-1} \approx 5 \text{ nsec}$ is revealed by Fig. 3 near $t = 10 \text{ nsec}$ and is caused by the rapid radial expansion of the breakdown plasma. Figure 4(a) graphs the

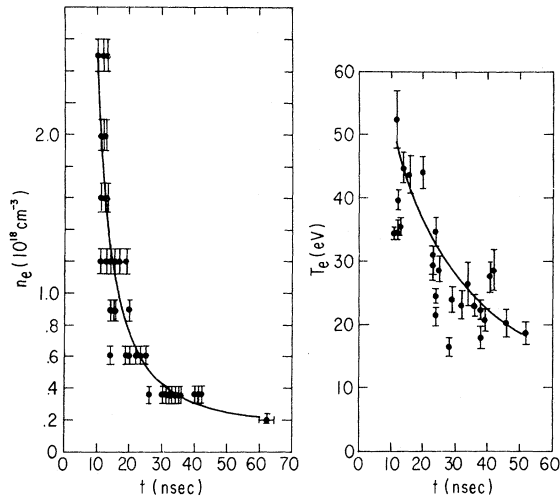


FIG. 3. $n_e(t)$ and $T_e(t)$ at the scattering volume; n_e is determined by 20° scattering and T_e by 150° scattering.

amplitude of the small-angle scattered signal versus density, assuming $\Delta\omega = \omega_{pe}$; a sharp increase in intensity occurs at $\Delta\omega = \omega_0/2$.

The stationary homogeneous-plasma thermal scattering level graphed in Fig. 4(a) is just

$$P_s = \frac{1}{2} P_i r_0^2 L_0 d\Omega (1 + \alpha^2)^{-1}, \quad (1)$$

where $d\Omega$ is the collected-light solid angle, $r_0^2 = 7.95 \times 10^{-26} \text{ cm}^2$, P_i is the ruby-laser power, P_s is the scattered power in the $\Delta\omega = \omega_{pe}$ wing, and α is calculated from Fig. 3. It was not possible to absolutely calibrate the system using Rayleigh scattering in a neutral gas, as the small ruby-laser focal spot always precipitated a gas breakdown. The spectrometer itself was absolutely calibrated, and the known losses between the scattering volume and spectrometer were incorporated into the thermal-level calculation. Since unknown losses such as small misalignments were not included, the thermal level graphed in Fig. 4(a) was always more than a factor of 2 larger than any observed signal amplitude for $\Delta\omega < \omega_0/2$. Nevertheless, the peak signal at $\Delta\omega = \omega_0/2$ is a factor of 7 above this level, clearly indicating the presence of the two-plasmon decay. A more realistic assessment of the expected scattering power is the graph in Fig. 4(a) for a time-varying inhomogeneous plasma, where it is assumed that at the time of scattering

$$n_e(z, t) = n_0 [1 + (z/L) - t/T], \quad (2)$$

where T is taken from Fig. 3. The resulting curve implies that virtually all of the scattering

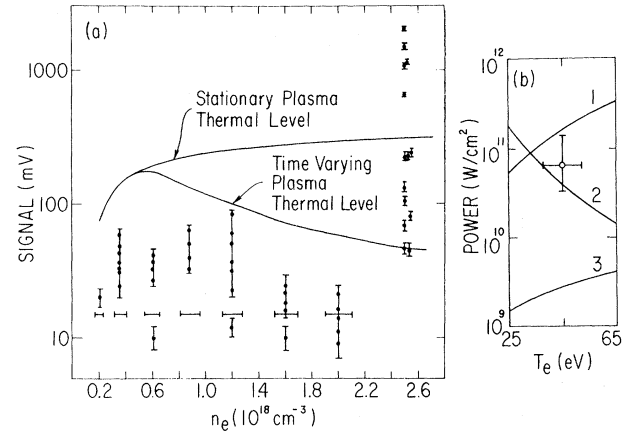


FIG. 4. (a) Scattering intensities vs n_e ; the horizontal bars indicate the channel widths. The upper curve is that of a homogeneous, stationary plasma and the lower curve takes into account time and space variations in n_e ; $\Delta\omega = \omega_0/2$ corresponds to $n_e = 2.5 \times 10^{18} \text{ cm}^{-3}$. (b) Threshold powers vs T_e for fixed $\Delta\vec{k}$; curve 1 is the absolute instability threshold, curve 2 is the homogeneous-plasma threshold, and curve 3 is the convective instability threshold. The bars indicate the experimental uncertainty of T_e and pump power at the time the instability is observed.

observations at $\omega_{pe} = \omega_0/2$ are nonthermal.

Figure 4(b) plots the threshold power versus T_e for parametric decay in a homogeneous collisional plasma,⁸ and for convective^{11,12} and absolute¹³ decay in an inhomogeneous collisionless plasma with $L = 2.5 \text{ mm}$, and where $\Delta\vec{k}$ is fixed by the scattering geometry. The bars indicate the experimental uncertainty in pump power and T_e when the instability is excited. Figure 4(b) indicates that the homogeneous plasma and convective thresholds are satisfied, but not the absolute threshold. If this decay were convective in nature, it would saturate at a level¹²

$$I \equiv \frac{\langle n_e^2(\Delta k, \Delta\omega) \rangle}{\langle n_e^2(\Delta k, \Delta\omega)_{\text{thermal}} \rangle} = \exp[(2\pi\gamma_0^2/V^2\kappa)(1 - 4\Gamma/\pi\gamma_0)], \quad (3)$$

where γ_0 is the instability growth rate, V its group velocity, $\kappa = (d/dz)(\sum_i k_{iz})$, Γ is the damping rate, and $\gamma_0 > \Gamma$. In estimating I , we must calculate the scattering-amplitude reduction factor $\delta = (\Delta z/L_0')(\Delta t/\tau)$, where τ is the ruby-laser pulse duration, Δz is the extent of the instability, Δt is the time duration of the instability in the scattering volume, and $L_0' = L_0 \cos 30^\circ$. Using Eq. (2), $\Delta t \approx (L_0'/L)T$, $T \approx 5 \text{ nsec}$, and interferom-

etry yields a value $|(1/n)/(dn/dz)|^{-1} = L = 2 \pm 1$ mm at $r = 0$. It may be shown that at resonance

$$\Delta\omega = \frac{-\omega_0}{2} \left(1 - \frac{9}{4} \frac{T_e}{m_e c^2} - \frac{9}{2} \frac{\Delta\vec{k} \cdot \hat{z}}{k_0} \frac{T_e}{m_e c^2} \right), \quad (4)$$

and that at any position $(\Delta\omega)^2 = \omega_{pe}^2 + 3\Delta k^2 T_e/m_e$. (The other sideband has $\omega' = \omega_0 + \Delta\omega$.) From Eq. (4) it can be shown that if we depart a distance Δz from resonance, the plasma wave detected at this Δz is at resonance at distance $\Delta z' \approx (2\Delta\vec{k} \cdot \hat{z}/k_0)\Delta z$ away. $\Delta z'$ is then just the width of the convective instability, which for our experimental parameters may be numerically calculated to be 30 ± 10 μm . Using these values, we may calculate I ; matching $\ln I$ to the exponent in Eq. (3) and letting the pump power be 10^{11} W/cm², we obtain $L = 2.7$ mm, in qualitative agreement with the experimentally determined value.

In conclusion, we have observed the parametric decay of CO₂-laser light into plasma waves at quarter-critical density; the amplitude and experimental parameters allow us to infer that this decay is convective. The technique of ruby-laser Thomson scattering in a CO₂-laser-heated gas-target plasma seems to hold great promise as a tool for diagnosing parametric turbulence of interest to laser-fusion schemes.

The authors are happy to acknowledge their valuable discussions with Dr. E. Valeo concern-

ing this work.

This work was supported by the U. S. Energy Research and Development Administration, Contract No. EY/76-C-02-3073.

^(a)Present address: Massachusetts Institute of Technology, Cambridge, Mass. 02139.

¹A. A. Offenberger, M. R. Cervenak, A. M. Yam, and A. W. Pasternak, *J. Appl. Phys.* **47**, 1451 (1976).

²John J. Turechek and Francis F. Chen, *Phys. Rev. Lett.* **36**, 720 (1976).

³B. Grek, H. Pépin, and F. Rheault, *Phys. Rev. Lett.* **38**, 898 (1977).

⁴Steven Jackel, Bruce Perry, and Moshe Lubin, *Phys. Rev. Lett.* **37**, 95 (1976).

⁵Steven Jackel, James Albritton, and Edward Goldman, *Phys. Rev. Lett.* **35**, 514 (1975).

⁶M. J. Forrest, P. D. Morgan, N. J. Peacock, K. Kuriaki, M. V. Goldman, and T. Rudolph, *Phys. Rev. Lett.* **37**, 1681 (1976).

⁷T. K. Chu and L. C. Johnson, *Phys. Fluids* **18**, 1460 (1975).

⁸E. Atlee Jackson, *Phys. Rev.* **153**, 235 (1967).

⁹L. C. Johnson and T. K. Chu, *Phys. Rev. Lett.* **32**, 517 (1974).

¹⁰Optical fibers supplied by Bell Laboratories.

¹¹Marshall N. Rosenbluth, *Phys. Rev. Lett.* **29**, 565 (1972).

¹²C. S. Liu, Marshall N. Rosenbluth, and Roscoe B. White, *Phys. Fluids* **17**, 1211 (1974).

¹³C. S. Liu and Marshall N. Rosenbluth, *Phys. Fluids* **19**, 967 (1976).

Electromagnetic Structure Resonances in Inhomogeneous Plasma Layers

F. J. Mayer, R. K. Osborn, D. W. Daniels, and J. F. McGrath

KMS Fusion, Ann Arbor, Michigan

(Received 21 September 1977)

Laser-light absorption and radiation forces are investigated for weakly collisional ($\nu/\omega \ll 1$), rigid, two-step plasma profiles in planar and spherical geometry. For the first step near critical density, the second step above critical, and appropriate step lengths, we find strong absorption even for weakly collisional plasmas. We show, however, that the radiation forces may not permit such profiles to persist in realistic, dynamic situations.

The subject of electromagnetic-wave absorption in high-density plasmas has received considerable attention recently^{1,2} because of its importance to the laser-driven-fusion program. It is well known that the electron density profile which is produced not only strongly affects the relative importance of various absorption mechanisms, but also affects the strength and direction of the ponderomotive force^{3,4} exerted on the ions through electrostatic coupling with the elec-

trons. The ponderomotive force has also received considerable attention recently⁵⁻⁷ in regard to self-consistent density profile formation; not all treatments, however, account for absorption and some are not rigorous. In this Letter, we examine the transverse electromagnetic wave interaction for two very simple inhomogeneous plasma layers, a two-step planar plasma layer and a two-step spherical layer. In these cases, the plasma is forced to be rigid, i.e., no plasma

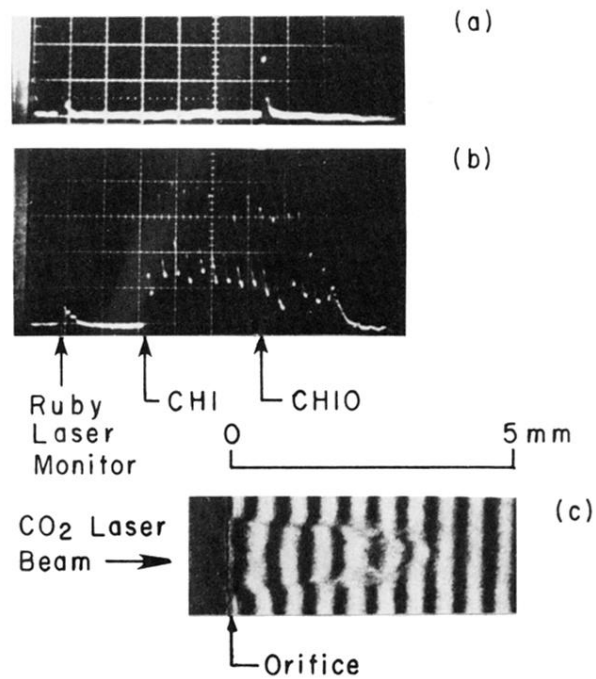


FIG. 2. Typical raw data. (a) 20° scattering spectrum exhibiting the instability and (b) is a typical 150° spectrum (1 division is 50 nsec). The photomultiplier gain in (a) is a factor of 8.8 less than in (b). The interferogram in (c) was taken simultaneously with an observation of the instability.